Picomole-scale characterization of protein stability and function by quantitative cysteine reactivity

Daniel G. Isom[1], Eyal Vardy[1], Terrence G. Oas, and Homme W. Hellinga[2]

Department of Biochemistry, Duke University, DUMC Box 3711, Durham, NC 27710

Edited by David Baker, University of Washington, Seattle, WA, and approved January 15, 2010 (received for review September 11, 2009)

The Gibbs free energy difference between native and unfolded states ("stability") is one of the fundamental characteristics of a protein. By exploiting the thermodynamic linkage between ligand binding and stability, interactions of a protein with small molecules, nucleic acids, or other proteins can be detected and quantified. Determination of protein stability can therefore provide a universal monitor of biochemical function. Yet, the use of stability measurements as a functional probe is underutilized, because such experiments traditionally require large amounts of protein and special instrumentation. Here we present the quantitative cysteine reactivity (QCR) technique to determine protein stabilities rapidly and accurately using only picomole quantities of material and readily accessible laboratory equipment. We demonstrate that QCR-derived stabilities can be used to measure ligand binding over a wide range of ligand concentrations and affinities. We anticipate that this technique will have broad applications in high-throughput protein engineering experiments and functional genomics.

conformational stability | thermal stability | ligand-binding affinity | linkage analysis | thiol protection

Biomolecular function is most often the consequence of interactions between molecules (enzymes with substrates, inhibitors, or activators; receptors with ligands; protein-protein networks; protein-DNA; and protein-RNA). Such functional interactions all affect protein stability by virtue of a thermodynamic linkage relationship between the Gibbs free energy of folding (ΔG_U) and binding free energy (ΔG_{bind}) of a ligand (L) to the native (N) or denatured (D) states (1–3)

$$\begin{array}{ccc} & \overset{\Delta^{\text{apo}}G_{\text{fold}}}{\rightleftarrows} & \\ \text{L} + \text{D} & & \text{N} + \text{L} \\ \Delta^{D}G_{\text{bind}}\ \downarrow\uparrow & & \downarrow\uparrow\ \Delta^{N}G_{\text{bind}} \\ \text{DL} & & \text{NL} \\ & \underset{\Delta^{L}G_{\text{fold}}}{\rightleftarrows} & \end{array} \qquad [1]$$

Macromolecular stability is therefore one of the most fundamental thermodynamic measures in biochemistry by quantitatively reporting on structure-function relationships to provide a universal monitor for biochemical function.

There are two distinct approaches for determining protein stability (4). The first measures the free energy of protein (un)folding under equilibrium conditions by assessing the fraction of the native state using spectroscopy, hydrodynamic observations, functional assays, or calorimetry. The second exploits the relationship between protein dynamics and stability by monitoring the differential reactivity of internal chemical groups in native and unfolded states. This second approach measures conformational free energies, which under appropriate conditions corresponds to global protein stability. Amide proton exchange is used most commonly to monitor such differential reactivity (5–9), but its widespread use to assess biological function typically is limited by the need for specialized instrumentation and relatively large amounts of protein. Recently, cysteine reactivity (10–14) and proteolysis (15) have emerged as alternative means to determine rates of protein (un)folding and estimate protein stabilities. Here we present a method, quantitative cysteine reactivity (QCR), in which protein stability is determined by monitoring the reactivity of cysteine residues buried in the hydrophobic core of proteins. This approach has the advantage over more traditional methods for measuring protein stability in that it requires only picomoles (nanograms) of protein, uses simple instrumentation accessible to any lab, can be reasonably high throughput, and can provide site-specific thermodynamic information. QCR can be used to determine apparent protein stabilities rapidly and accurately, construct Gibbs-Helmholtz stability profiles, measure ligand binding over a large range of ligand concentrations and affinities, and infer enzymatic activity without the need for developing a kinetic assay. Here we demonstrate these capabilities by characterizing three model proteins, *Staphylococcal* nuclease (SN), *Escherichia coli* ribose-binding protein (ecRBP) and *E. coli* maltose-binding protein (ecMBP), mutated to contain single, buried cysteine residues.

Results and Discussion

Measuring Conformational Free Energies by QCR. The QCR experiment is designed to determine the Gibbs free energy of global protein unfolding by measuring the reactivity of wild-type or mutant cysteines buried in a hydrophobic core. Here we demonstrate the QCR approach in three model proteins (SN, ecRBP, and ecMBP) mutated to contain cysteine probes located in internal microenvironments that flank ligand-binding sites, but do not contact directly bound metals, inhibitors, or ligands (see Fig. S1). These mutant proteins were produced in 200 μL batches by cell-free coupled transcription and translation in *E. coli* extract. Following affinity purification, which typically yields 0.4 to 1 μg of protein, the reactivity of the buried cysteines was determined by timed endpoint analysis experiments in which the modified protein species were separated by gel electrophoresis and quantified by densitometry (Fig. 1). This approach requires approximately 0.5 picomoles (~10 nanograms) of protein per time point and can use a variety of thiol-reactive reagents that alter electrophoretic mobility or are highly fluorescent.

The QCR method exploits the conformational fluctuations of a protein to measure conformational free energy. Cysteines that are protected in the folded ensemble can be modified by thiol-reactive probe only by complete exposure to bulk solvent by transient unfolding reactions, as described by a two-step reaction scheme (5, 13)

$$\text{Closed-SH} \underset{k_{\text{close}}}{\overset{k_{\text{open}}}{\rightleftarrows}} \text{Open-SH} \overset{k_{\text{int}}}{\rightarrow} \text{Open-S-Labeled}. \qquad [2]$$

Unfolding free energies (ΔG_U) can be determined under EX2 conditions (where $k_{\text{close}} \gg k_{\text{int}}$) by measuring k_{label}, the rate

Author contributions: D.G.I. and E.V. designed research; D.G.I. and E.V. performed research; D.G.I., E.V., and T.G.O. analyzed data; and D.G.I., T.G.O., and H.H. wrote the paper.

The authors declare no conflict of interest.

This article is a PNAS Direct Submission.

[1]D.G.I. and E.V. contributed equally to this work.

[2]To whom correspondence should be addressed. E-mail: hwh@biochem.duke.edu.

This article contains supporting information online at www.pnas.org/cgi/content/full/0910421107/DCSupplemental.

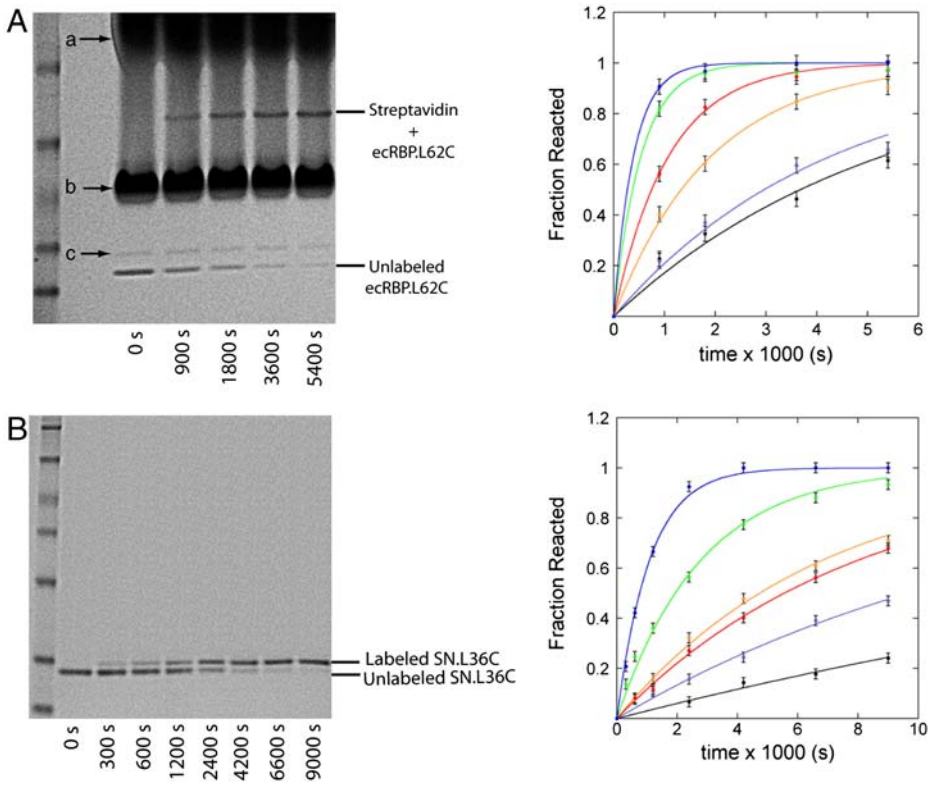

Fig. 1. Representative QCR experiments for ecRBP and SN. (*A*) SDS-PAGE of time-dependent modification of ecRBP variant L62C with 1 mM IAM-biotin at 47.1 °C, pH 7.6 (*left*) (labeling times indicated for lanes 2–6). Streptavidin was used to alter the electrophoretic mobility of the labeled protein (streptavidin bands indicated by a, b, and c). Unlabeled fractions were quantified by densitometry and fit with a single exponential to obtain reaction rates (*right*) at different temperatures (54.6 °C, blue; 51.7 °C, green; 48.9 °C, red; 47.1 °C, orange; 45.2 °C, purple; 44.5 °C, black); corresponding reaction rates are 2.6×10^{-3}, 1.9×10^{-3}, 9.3×10^{-4}, 5.2×10^{-4}, 2.6×10^{-4}, and 2.0×10^{-4} s^{-1}, respectively. Error bars represent the estimated uncertainty of the integrated band intensities (~2%). (*B*) Labeling of SN variant L36C with IAM-biotin at 35.3 °C, pH 7.6 (*left*). The (un)labeled forms migrate differently in the gel, enabling ratiometric quantification to obtain reaction rates (*right*) at different temperatures (38.3 °C, blue; 35.3 °C, green; 32.3 °C, red; 29.3 °C, orange; 26.3 °C, purple; 23.3 °C, black); corresponding reaction rates are 9.2×10^{-4}, 3.6×10^{-4}, 1.2×10^{-4}, 1.5×10^{-4}, 7.2×10^{-5}, and 3.1×10^{-5} s^{-1}, respectively. At 29.3 °C, 26.3 °C, and 23.3 °C, k_{int} and k_{label} were manipulated by increasing the concentration of IAM-biotin from 1 mM to 3.16 mM.

constant for labeling a protected cysteine at a specified concentration of thiol probe [P] (5)

$$k_{\text{label}} = \frac{k_{\text{open}}k_{\text{int}}}{(k_{\text{open}} + k_{\text{close}} + k_{\text{int}})} \underset{\text{EX2}}{\cong} \frac{k_{\text{open}}k_{\text{int}}}{(k_{\text{open}} + k_{\text{close}})} = \frac{k_{\text{int}}}{(1 + e^{\Delta G_U/RT})}, \quad [3]$$

where ΔG_U is related to the closing (k_{close}) and opening (k_{open}) reaction as $\Delta G_U = RT \ln k_{close}/k_{open}$, and k_{int} is the product of [P] and the biomolecular rate constant for the reaction of an unprotected cysteine ($k_{int} = k[P]$). Values for k_{int} can be obtained from the reactivity of unprotected cysteine residues in model compounds or unfolded proteins for the accurate determination of ΔG_U (see *Methods*). Rearrangement of Eq. **3** yields conformational free energy

$$\Delta G_U = RT \ln\left(\frac{k_{\text{int}} - k_{\text{label}}}{k_{\text{label}}}\right). \quad [4]$$

A buried cysteine can be labeled as a result of local, subglobal, or global unfolding transitions. The predominant mechanism of cysteine modification can be converted from local or partial unfolding to global unfolding by setting up conditions under which global stability is diminished (e.g. by addition of denaturation or by increasing temperature) (16, 17). We refer to the range of conditions under which access to global unfolding predominates as the global unfolding window of observation (GUWO) (see Fig. 2).

To ensure that the buried cysteines report global free energies (i.e. ΔG_U), QCR experiments are always performed within a GUWO. We have chosen to use temperature to access the GUWO and measure global unfolding free energies as a function of temperature ($\Delta G_U(T)$), described by the Gibbs-Helmholtz relationship (18)

$$\Delta G_U(T) = \Delta H_m\left(1 - \frac{T}{T_m}\right) - \Delta C_p\left((T_m - T) + T \ln\frac{T}{T_m}\right), \quad [5]$$

where ΔH_m is the enthalpy of unfolding, ΔC_p the change in heat capacity of unfolding, and T_m the midpoint of thermal denaturation, readily determined by QCR as the temperature at which $k_{int} = 2k_{label}$. The temperature range over which observations can be made is determined by the limits where differences between k_{label} and k_{int} exceed experimental error, EX2 conditions prevail, and the GUWO is present (see Fig. 2). This range comprises a small portion of a Gibbs-Helmholtz curve. Consequently, values for ΔH_m and ΔC_p derived from a fit of the temperature dependence of ΔG_U are usually underdetermined (19, 20), and values for ΔC_p must be assigned a priori to derive reasonable estimates for ΔH_m and T_m from stabilities measured within the GUWO.

Using a total of only ~12.5 picomoles of protein (~2.5 picomoles or ~50 nanograms per temperature point), Gibbs-Helmholtz profiles were determined for two cysteine mutants of SN and ecRBP (Fig. 3). Derived values for ΔH_m and T_m were relatively insensitive to ΔC_p values within the range of

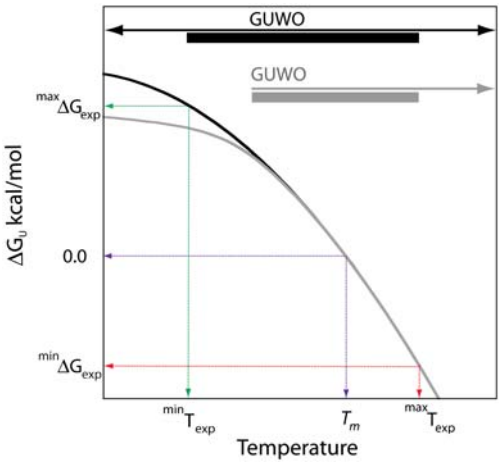

Fig. 2. Three factors determine the temperature range at which global unfolding free energies (ΔG_U) can be determined by quantitative cysteine reactivity. The first limits are set by the accuracy of the measurement of the labeling rate constants: an upper limit occurs at a temperature ($^{max}T_{exp}$) and free energy ($^{min}\Delta G_{exp}$) at ~10 °C above T_m (red-dashed arrows) where the difference of k_{label} and k_{int} is within experimental error; a lower limit occurs at a temperature ($^{min}T_{exp}$) and free energy ($^{max}\Delta G_{exp}$) at ~10–20 °C below T_m (green-dashed arrows) where increased stability sufficiently reduces k_{label} (Eqs. **3** and **4**) such that it appears to be independent of temperature within experimental error. The second limit is set in some cases where the mechanism of cysteine protection (i.e. local or global unfolding) is dependent on temperature. Such cases manifest themselves as a deviation of the observed temperature dependence of ΔG_U from that expected for global unfolding. It is well established that global unfolding conditions prevail within ~10–20 °C of T_m (16, 17), which we refer to as the global unfolding window of observation. The black line illustrates a case in which there is no such switch (modeled by Eq. **5**) and the GUWO extends over the entire temperature range; the gray line represents switching between global and local unfolding with a concomitant temperature limit for the GUWO (modeled by Eq. 12 of ref. 6). The third limit is set at a point where EX1 conditions prevail and k_{close} no longer exceeds k_{int} (not illustrated). This may occur as stability is diminished (ΔG_U < 1 kcal/mol) or if the concentration of thiol probe [P] is too high. Loss of EX2 conditions is manifested as a loss of the linear dependence of k_{label} on [P] and can be remedied by reducing [P]. The overall temperature range at which observations can be made is the intersection of all three of these conditions (black and gray bars).

2–5 kcal mol^{-1} K^{-1}, which is consistent with previous experimentally determined values for proteins in general (21–23). All four cysteine mutants are thermally destabilized: the apparent T_m values of SN variants F34C (40 ± 1 °C) and L36C (39 ± 1 °C) are ~13.0 °C below wild-type (53.0 °C) (24); the apparent T_m values of ecRBP variants L62C (54 ± 1 °C) and A188C (56 ± 1 °C) are ~8 °C below wild-type (62.6 °C) (25). The extrapolated ΔG^o_U at 20 °C for SN mutants F34C and L36C, using ΔH_m values of 72 ± 1 and 71 ± 1 kcal mol^{-1}, respectively, is 2.7± 0.1 kcal mol^{-1} and 2.6 ± 0.1 kcal mol^{-1}, whereas the stability of wild-type SN reported by chemical denaturation is 5.5 ± 0.1 kcal mol^{-1} (26). Similarly, the ΔG^o_U at 25 °C for ecRBP mutants L62C and A188C, using ΔH_m values of 81 ± 2 and 91 ± 4 kcal mol^{-1}, respectively, is 3.2 ± 0.1 kcal mol^{-1} and 4.1 ± 0.1 kcal mol^{-1}, whereas the stability of wild-type reported by chemical denaturation is 5.9 ± 0.4 kcal mol^{-1} (27). This decrease in stability caused by the introduction of cysteine is typical for mutations in the hydrophobic core of these (26, 28) and other (29) proteins.

Measuring Ligand Affinity by Linkage Analysis of Protein Stability. The modulation of protein stability by binding of metals, ligands, activators, inhibitors, substrates, nucleic acid, or other proteins can be used to measure binding affinities within a GUWO. For a protein with a single binding site, the free energy of ligand binding is described by

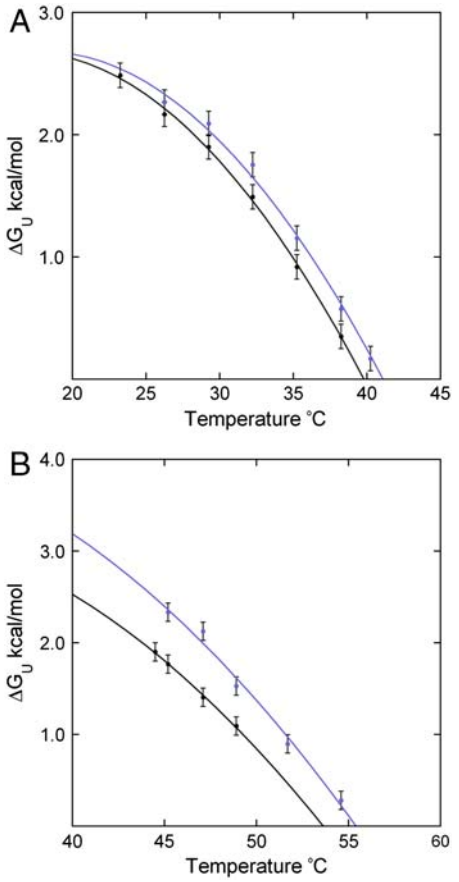

Fig. 3. Temperature dependence of ΔG_U determined by QCR for (*A*) SN variants F34C (purple) and L36C (black), and (*B*) ecRBP variants L62C (black) and A188C (purple). Solid lines indicate a fit to a Gibbs-Helmholtz profile (Eq. **5**) using a fixed ΔC_p of 3 kcal mol^{-1} K^{-1}. Error bars represent the error of three independent experiments at select temperatures.

$$\Delta G_{\text{bind}} = RT \ln P = RT \ln\left(1 + \frac{[L]}{K_D}\right), \qquad [6]$$

where P is the binding polynomial (1–3), $[L]$ the total ligand concentration, and K_D the apparent dissociation constant of the ligand. For proteins with multiple ligand-binding sites, P is expanded (*SI Text*). By thermodynamic linkage (3, 30) any change in ΔG_U caused predominantly by ligand binding (Eq. **1**) is

$$\Delta G_{\text{bind}} = \Delta\Delta^L G_U = \Delta^L G_U - \Delta^{\text{apo}} G_U, \qquad [7]$$

where $\Delta^L G_U$ and $\Delta^{\text{apo}} G_U$ are the stability of the protein in the presence or absence of ligand, respectively. Eq. **7** is used to obtain apparent K_D values from either the ligand dependence of $\Delta\Delta G_U$ (by curve fitting) or from a single measurement of $\Delta\Delta G_U$.

Both ecRBP and ecMBP have a single ligand-binding site located within the interface between their N-terminal and C-terminal domains. With ~10 picomoles (~200 nanograms) of protein, binding affinities were determined by QCR experiments using two independent cysteine reporters introduced into each domain. ecRBP variants L62C (N-terminal domain) and A188C (C-terminal domain) report ribose-binding affinities of 1.5 ± 0.2 μM (at 48.9 °C) and 1.8 ± 0.1 μM (at 54.6 °C), respectively (Fig. 4*A*); ecMBP variants T157C (C-terminal domain) and S263C (N-terminal domain) report maltose-binding affinities of 8.0 ± 0.2 μM and 11.8 ± 0.8 μM, respectively at 63.3 °C (Fig. 4*B*).

Proteins that bind more than one ligand, either independently or synergistically, have a more complex free energy landscape that involves a number of different ligand-bound species (*SI Text*). Here, we demonstrate how QCR can be used to characterize

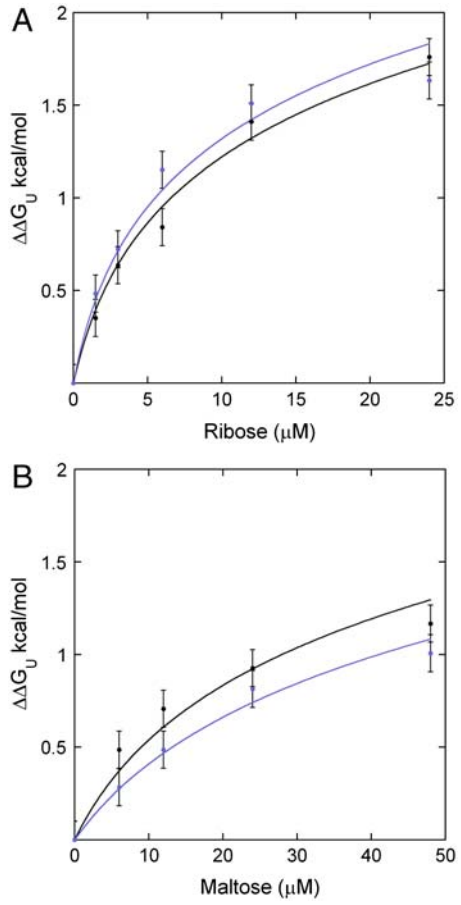

Fig. 4. Ligand concentration dependence of $\Delta\Delta G_U$ for (*A*) ecRBP variants L62C (purple) at 48.9 °C and A188C (black) at 54.6 °C, and for (*B*) ecMBP variants T157C (black) and S263C (purple) at 63.3 °C. The solid lines represent the fit of Eq **7** to the data to obtain K_D values. Error bars correspond to the propagated uncertainty of two combined ΔG_U measurements.

the binding of a calcium ion (Ca^{2+}) and a 5′-monophosphate inhibitor (pdTp) to SN. By themselves, Ca^{2+} and pdTp bind to SN with affinities of ~500 μM and ~90 μM (31). Using ~5 picomoles (~100 nanograms) of protein, the K_D values of each binary complex was determined by QCR (Fig. 5*A*). The increase in stability of SN/L36C in the presence of 1 mM Ca^{2+} or 50 μM pdTp is 0.6 ± 0.1 and 0.7 ± 0.1 kcal/mol, which corresponds to apparent K_D values of 600 ± 200 μM and 23 ± 4 μM, respectively. Binding of Ca^{2+} and pdTp is synergistic, as each exhibits a greater affinity (~2 μM) for SN in the presence of the other (31). Consequently, a 2:1 molar solution of Ca^{2+}:pdTp can be treated thermodynamically as a single, binary ligand Ca^{2+}-pdTp. Using ~10 picomoles (~200 nanograms) of protein, the affinity of Ca^{2+}-pdTp for SN variants F34C and L36C was determined to be 4.8 ± 0.2 μM and 2.2 ± 0.1 μM, respectively, at 35.3 °C (Fig. 5*B*).

Inferring Enzyme Activity by QCR. Binding of substrates and products also affects enzyme stability in a detectable manner (32). QCR therefore provides a means to infer enzymatic activity within a GUWO using only picomole quantities of protein without having to devise a reaction-specific kinetic assay. We demonstrate this approach using SN, a 5′-phosphodiesterase that hydrolizes single- and double-stranded DNA and RNA. It selectively cleaves the phosphodiester bond between the phosphate and 5′-hydroxyl, producing short 3′-derived oligonucleotides (which do not bind to SN) and 5′-derived mononucleotides (which bind to and inhibit SN) (33). In the absence of calcium,

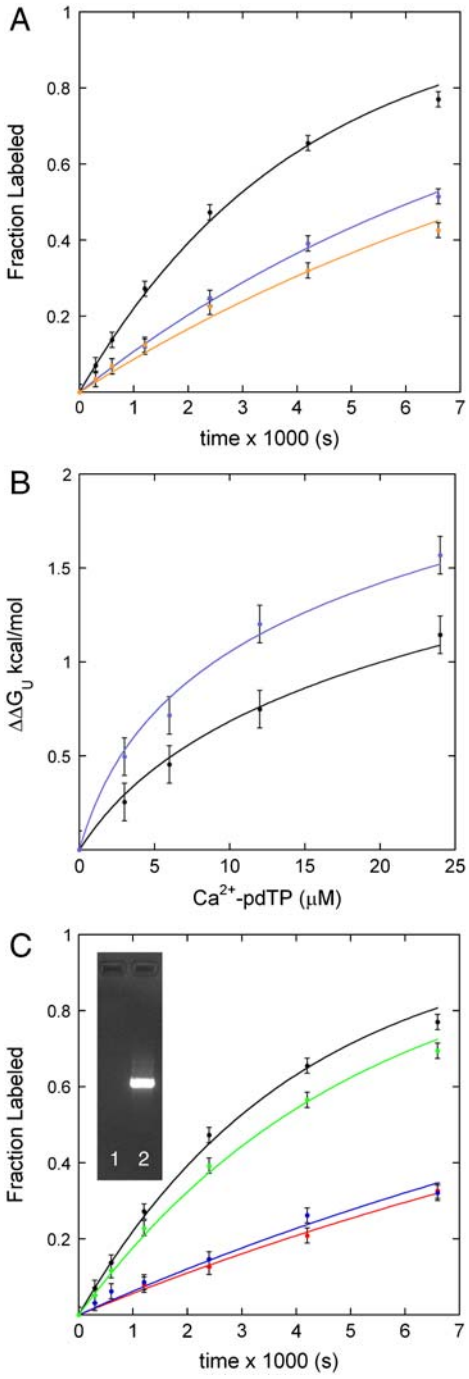

Fig. 5. Effect of ligands and substrate on SN stability. (*A*) QCR experiments for SN variant L36C in the absence (black) and presence of 1 mM Ca^{2+} (purple) or 50 μM pdTp (orange) at 35.3 °C. Observed rate constants of 3.0×10^{-4}, 1.2×10^{-4}, and 9.2×10^{-5} s^{-1}, respectively, correspond to $\Delta\Delta G_U$ values of 0.6 ± 0.2 and 0.7 ± 0.2 kcal mol^{-1}. (*B*) Dependence of $\Delta\Delta G_U$ on a 2:1 molar ratio of Ca^{2+} and pdTp for SN variants F34C (black) and L36C (purple) fit with Eq. **7** to obtain K_D values. (*C*) QCR experiments at 35.3 °C for SN variant L36C in the absence of substrate (black) and 4.7 μM single-stranded DNA (green), 4.7 μM single-stranded DNA with 1 mM Ca^{2+} (blue), and 12 μM of a 2:1 molar ratio of Ca^{2+} and pdTp (red). Observed rate constants of 3.0×10^{-4}, 2.8×10^{-4}, 7.5×10^{-5}, and 5.9×10^{-5} s^{-1}, respectively, correspond to $\Delta\Delta G_U$ values of 0.1 ± 0.2, 0.9 ± 0.2, and 1.0 ± 0.2 kcal mol^{-1}. The L36C mutant is enzymatically active (inset; 1% agarose gel): 1.5 kb double-stranded DNA fragment (lane 2) digested completely (lane 1) by incubation with 0.05 μM SN/L36C at 20 °C for 10 min in a buffer of 1 mM Ca^{2+}, 25 mM MOPS, 100 mM KCl, and pH 7.6. The k_{cat}, k_{cat}/K_m, and K_m of SN for canonical substrate (double-stranded salmon sperm DNA) are ~90 s^{-1}, 2×10^6 M^{-1} s^{-1}, and ~50 μM, respectively, at pH 7 (38).

SN is inactive and the binding of substrate alone can be measured by QCR. Addition of 4.7 μM substrate DNA in the absence of calcium produces no observable effect on the stability reported by Cys-36 (Fig. 5*C*). Following addition of 1 mM calcium, the substrate DNA is rapidly degraded (inset Fig. 5*C*), and the QCR-determined stability of SN/L36C is increased by 0.9 ± 0.1 kcal mol^{-1}, corresponding to an apparent binding affinity of 1.4 ± 0.4 μM, which is nearly identical to the affinity of the inhibitor pdTp in the presence of 1 mM Ca^{2+} and therefore is presumably due to the effect of product binding.

Conclusions

The increasing trend of biological research towards more quantitative descriptions and models has generated an urgent demand for simple and accessible techniques that can provide thermodynamic data on such fundamental properties as protein stability and ligand binding. We have demonstrated that quantitative cysteine reactivity can be used to determine protein stability using only picomole quantities of material (nanograms for an average-sized protein), readily accessible gel electrophoresis equipment, and freely available gel analysis software. Furthermore, QCR assesses stability at low protein concentrations, thereby minimizing aggregation, a common problem in stability measurements made by less sensitive methods. QCR exploits the fundamental relationship between protein flexibility and stability by monitoring the differential reactivity of internal chemical groups in the native and unfolded state, first pioneered by hydrogen exchange (HX) as the experimental observation (5). Unlike HX, QCR observations are always obtained within the GUWO (~10–15 °C of T_m), where global unfolding events dominate and where the reported energetics correspond to global unfolding free energies.

QCR can be used to investigate many aspects of biological function that are linked to protein stability. For instance, protein-ligand interactions can be readily identified and quantified through the fundamental thermodynamic linkage relationships between ligand binding and protein stability. This analysis can be extended to infer enzymatic activity by monitoring changes in stability in the presence of substrate, product (produced in the course of the reaction), or inhibitors. Such observations by themselves do not provide direct evidence of catalytic activity but can be invaluable for establishing substrate specificity and inhibitor identity, even in the absence of reaction-specific kinetic assays. The ability to obtain thermodynamic measurements with small amounts of material and simple instrumentation enables potential widespread application and adaptation of the QCR technique for protein characterization, including protein engineering experiments and functional genomic studies that require the thermodynamic characterization of a large number of variants.

Methods

Cell-Free Expression and Purification of Proteins Encoded by Synthetic Genes. The wild-type proteins and cysteine variants were produced by cell-free in vitro transcription and translation (TnT) using an *E. coli* extract from Bl21 Star (DE3) (Invitrogen; C6010-03) (34) programmed with a synthetic linear DNA fragment that was constructed using automated, PCR-mediated gene assembly (35). The synthetic gene sequences (see *SI Fabricated Synthetic Gene Sequences (ORFs)*) comprise a 5′ T7-promoter, a 5′ ribosome binding site, and a 3′ T7-terminator flanking an open reading frame whose DNA sequence was optimized for protein expression using a computational algorithm that manipulates mRNA structure (Allert, Cox, and Hellinga, in preparation). All proteins contain a C-terminal FLAG-affinity tag (GGSDYKDDDDK) (36) for purification. The version of ecRBP used in this study has the additional mutation T3W. Approximately 2 μg of DNA was added to 200 μL TnT extract and incubated at 30 °C for 2 h. Proteins were purified using FLAG-affinity beads (Sigma; F2426): beads were preblocked for 2 h (Starting Block; Thermo Scientific; 37543) and washed with Tris buffered saline (TBS) (25 mM Tris, 150 mM NaCl, pH 7.4). Next, 100 μL of TnT extract was combined with 1 mL Flag beads ($A_{600} = 0.25$), incubated at 4 °C (15 min with end-over-end mixing), washed twice with 1 mL of TBS, and eluted with 3x-FLAG peptide (Sigma; F4799) buffer (25 mM MOPS, 100 mM KCl, 150 μM 3x-FLAG peptide, and pH 7.6). Purified proteins were used directly in QCR experiments.

The QCR Experiment. The rate of labeling of internal cysteine residues was measured by reacting 30–50 μL of ~0.1 μM protein sample (i.e., ~3–5 picomoles of protein) with IAM-biotin (EZ-link Iodoacetyl-PEG$_2$-Biotin; Pierce; 21334) in excess (1 mM unless otherwise stated) at constant temperature (25 mM MOPS, 100 mM KCl and pH 7.6). Five μL aliquots were removed at fixed time intervals and quenched by addition of 2 μL 2 M β-mercaptoethanol (Sigma; M6250). Following addition of 5 μL LDS-buffer (Invitrogen; NP0007) and heating for 2 min at 85 °C, (un)labeled protein species were resolved by SDS-PAGE (Novex 4–12% Bis-Tris Gels; Invitrogen; NP0321). Observed gel shifts of the biotinylated species are caused either by slight differences in conformation between the (un)labeled species (Fig. 1*B*) or, more typically, by addition of 4 μL of 40 mg/mL streptavidin (Pierce; 21125) *after* heating (Fig. 1*A*). Following staining with GelCode Blue Stain reagent (Thermo Scientific; 24592), gel images were digitized and band intensities quantified by densitometry [ImageJ (37)] and fit to a single exponential to derive k_{label} (Tables S1 and S2). When designing QCR experiments, it is important to consider the degradation of the iodoacetyl moiety of IAM-biotin, which is dependent on time, exposure to light, and temperature. At temperatures less than ~65 °C, we have observed this effect to be negligible over the time-course of ~2 hours. At higher temperatures the degradation of IAM-biotin must be taken into account, primarily by limiting the labeling reaction to less than ~90 min.

It is important to note that Eq. **4** applies only if the labeling conditions are fully in the EX2 limit. As labeling reagent concentration increases, k_{int} increases concomitantly and eventually k_{int} will become equal to or greater than k_{close}. Under these conditions, the observed labeling rate is determined solely by k_{open} and k_{label} and is no longer a measure of stability. The reagent concentration and environmental conditions (i.e. pH and temperature) at which EX2 conditions no longer apply varies according to the (un)folding kinetics of the protein. A simple test of reaction mechanism is to change reagent concentration and remeasure the kinetics: EX2 conditions are satisfied if the change in the observed labeling rate is proportional to the change in reagent concentration (Fig. S3).

Determining Intrinsic Reaction Rates of Unprotected Cysteines. The iodoacetyl moiety of IAM-biotin reacts primarily with free thiolate to form a stable thioether bond. Because thiolate is the predominant reactive species, the reaction rate is dependent on the pK_a of cysteine (~8.6) relative to solution pH (which is set to 7.6). It is important to note that the k_{int} values reported here are only valid for pH 7.6. k_{int} was determined for an unprotected cysteine by reacting IAM-biotin with *L*-glutathione (GSH) (Sigma; G4251) and monitoring the absorbance of the liberated iodide ion ($\varepsilon_{226} = 12,600$ M^{-1} cm^{-1} at 226 nm) as a function of time. Second-order rate constants for the reaction of IAM-biotin with GSH were measured under pseudo-first-order conditions at 25 °C, 35 °C, 45 °C, and 55 °C (80 μM IAM-biotin, 800 μM GSH, 25 mM MOPS, 100 mM KCl, and pH 7.6) and analyzed in terms of the Arrhenius equation (Fig. S2). The slope ($-E_a/R$) and preexponential factor ($\ln A$) were found to be $-8.2 \times 10^3 \pm 0.1 \times 10^3$ and 27.1 ± 0.5 s^{-1}, respectively, enabling k_{int} to be calculated at any temperature. k_{int} values derived from unfolded proteins were in direct agreement with the GSH-derived k_{int} values.

ACKNOWLEDGMENTS. This work was supported by the NIH Director's Pioneer Award (5DPI OD000122) and the Homeland Security Advanced Research Projects Agency (HSH ODC-08-C-00099).

1. Wyman J (1964) Linked functions and reciprocal effects in hemoglobin: A second look. *Adv Protein Chem* 19:223–286.
2. Schellman JA (1975) Macromolecular Binding. *Biopolymers* 14(5):999–1018.
3. Wyman J, Gill SJ (1990) *Binding and Linkage* (University Science Books, Mill Valley, CA) p 330.
4. Huyghues-Despointes B, Pace CN, Englander SW, Scholtz JM (2001) *Protein Structure, Stability, and Folding* (Humana Press Inc, Totowa, NJ).
5. Hvidt A, Neilson SO (1966) Hydrogen exchange in proteins. *Adv Protein Chem* 21:287–386.
6. Bai YW, Milne JS, Mayne L, Englander SW (1994) Protein stability parameters measured by hydrogen-exchange. *Proteins* 20(1):4–14.
7. SwintKruse L, Robertson AD (1996) Temperature and pH dependences of hydrogen exchange and global stability for ovomucoid third domain. *Biochemistry-US* 35(1):171–180.

8. Huyghues-Despointes BMP, Scholtz JM, Pace CN (1999) Protein conformational stabilities can be determined from hydrogen exchange rates. *Nat Struct Biol* 6(10):910–912.
9. Ghaemmaghami S, Fitzgerald MC, Oas TG (2000) A quantitative, high-throughput screen for protein stability. *Proc Natl Adac Sci USA* 97(15):8296–8301.
10. Ha JH, Loh SN (1998) Changes in side chain packing during apomyoglobin folding characterized by pulsed thiol-disulfide exchange. *Nat Struct Biol* 5(8):730–737.
11. Feng ZY, Butler MC, Alam SL, Loh SN (2001) On the nature of conformational openings: Native and unfolded-state hydrogen and thiol-disulfide exchange studies of ferric aquomyoglobin. *J Mol Biol* 314(1):153–166.
12. Sridevi K, Udgaonkar JB (2002) Unfolding rates of barstar determined in native and low denaturant conditions indicate the presence of intermediates. *Biochemistry-US* 41(5):1568–1578.
13. Jha SK, Udgaonkar JB (2007) Exploring the cooperativity of the fast folding reaction of a small protein using pulsed thiol labeling and mass spectrometry. *J Biol Chem* 282(52):37479–37491.
14. Silverman JA, Harbury PB (2002) The equilibrium unfolding pathway of a $(\beta/\alpha)_8$ barrel. *J Mol Biol* 324(5):1031–1040.
15. Park C, Marqusee S (2004) Probing the high energy states in proteins by proteolysis. *J Mol Biol* 343:1467–1476.
16. Bai YW, Englander JJ, Mayne L, Milne JS, Englander SW (1995) *Methods in Enzymology,* ed Johnson ML (Academic, New York), Vol 259, pp 344–356.
17. Milne JS, Xu YJ, Mayne LC, Englander SW (1999) Experimental study of the protein folding landscape: Unfolding reactions in cytochrome c. *J Mol Biol* 290(3):811–822.
18. Privalov P (1979) Stability of proteins. *Adv Protein Chem* 33:167–241.
19. Chaires JB (1997) Possible origin of differences between van't Hoff and calorimetric enthalpy estimates. *Biophys Chem* 64(1-3):15–23.
20. Prabhu NV, Sharp KA (2005) Heat capacity in proteins. *Ann Rev Phys Chem* 56:521–548.
21. Gomez J, Hilser VJ, Xie D, Freire E (1995) The heat-capacity of proteins. *Proteins* 22(4):404–412.
22. Razvi A, Scholtz JM (2006) Lessons in stability from thermophilic proteins. *Protein Sci* 15(7):1569–1578.
23. Rees D, Robertson AD (2001) Some thermodynamic implications for the thermostability of proteins. *Protein Sci* 10:1187–1194.
24. Talla-Singh D, Stites WE (2008) Refinement of noncalorimetric determination of the change in heat capacity, ΔC_p, of protein unfolding and validation across a wide temperature range. *Proteins* 71(4):1607–1616.
25. Prajapati RS, Indu S, Varadarajan R (2007) Identification and thermodynamic characterization of molten globule states of periplasmic binding proteins. *Biochemistry-US* 46(36):10339–10352.
26. Green SM, Meeker AK, Shortle D (1992) Contributions of the polar, uncharged amino-acids to the stability of Staphylococcal nuclease—evidence for mutational effects on the free-energy of the denatured state. *Biochemistry-US* 31(25):5717–5728.
27. Prajapati RS, et al. (2007) Thermodynamic effects of proline introduction on protein stability. *Proteins* 66(2):480–491.
28. Kim JS, Kim H (1996) Stability and folding of a mutant ribose-binding protein of Escherichia coli. *J Protein Chem* 15(8):731–736.
29. Bava KA, Gromiha MM, Uedaira H, Kitajima K, Sarai A (2004) ProTherm, version 4.0: Thermodynamic database for proteins and mutants. *Nucleic Acids Res* 32:120D–121D.
30. Waldron TT, Murphy KP (2003) Stabilization of proteins by ligand binding: Application to drug screening and determination of unfolding energetics. *Biochemistry-US* 42(17):5058–5064.
31. Serpersu EH, Shortle DR, Mildvan AS (1986) Kinetic and magnetic-resonance studies of effects of genetic substitution on Ca^{2+}-liganding amino-acid in Staphylococcal nuclease. *Biochemistry-US* 25(1):68–77.
32. Pace CN, McGrath T (1980) Substrate stabilization of lysozyme to thermal and guanidine-hydrochloride denaturation. *J Biol Chem* 255(9):3862–3865.
33. Cuatrecasas P, Fuchs S, Anfinsen CB (1967) Catalytic properties and specificty of extracellular nuclease of Staphylococcus aureus. *J Biol Chem* 242(7):1541–1547.
34. Jewett M, Swartz J (2004) Mimicking the Escherichia coli cytoplasmic environment activates long-lived and efficient cell-free protein synthesis. *Biotechnol Bioeng* 86(1):19–26.
35. Cox JC, Lape J, Sayed MA, Hellinga HW (2007) Protein fabrication automation. *Protein Sci* 16(3):379–390.
36. Hopp T, et al. (1988) A short polypeptide marker sequence useful for recombinant protein identification and purification. *Nat Biotechnol* 6(10):1204–1210.
37. Rasband W (1997–2009) *ImageJ* (U.S. National Institutes of Health, Bethesda, Maryland).
38. Hale S, Poole L, Gerlt J (1993) Mechanism of the reaction catalyzed by Staphylococcal nuclease: Identification of the rate-limiting step. *Biochem J* 32(29):7479–7487.